Journal of Sound and Vibration 623 (2026) 119550

Contents lists available at ScienceDirect

Journal of Sound and Vibration

journal homepage: www.elsevier.com/locate/jsvi

Rapid Communications

Electromagnetic and structural dynamic coupling in a two-degree-of-freedom system

Mikel Brun *, Fernando Cortés, María Jesús Elejabarrieta

Department of Mechanics, Design and Industrial Management, University of Deusto, Avda. de las Universidades 24, 48007 Bilbao, Spain

ARTICLE INFO

Keywords:
Induced current damping
Structural dynamics
Coupling matrix
Magnetic fields
Frequency response
Time response
Energy transfer

ABSTRACT

Induced current damping is widely used to mitigate vibrations in mechanical systems. Conventional formulations of electromagnetic force matrices often assume constant, linear, or frequency-dependent coefficients. In a recent study, the authors observed that when a cantilever beam subjected to bending or torsional vibrations is exposed to an external magnetic field in multiple directions, an unexpected coupling between vibration modes occurs. This phenomenon suggests that existing models may be insufficient to capture the complete dynamic behaviour resulting from induced currents. Consequently, this Rapid Communication investigates this coupling effect using a simplified two-degree-of-freedom system under an external magnetic field. The effect of this magnetic field implies a coupling between the two degrees of freedom of the system, characterised by a symmetric matrix containing both dissipative and coupling terms. A frequency response analysis reveals a particular behaviour at resonance when the two degrees of freedom are coupled, which occurs only when the magnetic field acts simultaneously in both directions. In this case, increasing the magnetic field magnitude mitigates one vibration mode while amplifying the other. In the time domain, the analysis of the mechanical energy evolution of each degree of freedom reveals how energy is transferred between the two degrees of freedom as the system dissipates energy. These findings highlight the necessity of explicitly incorporating magnetic field orientation and magnitude into electromagnetic force matrices to accurately predict the coupling effects. The results serve as a foundation supporting future studies on more complex multi-degree-of-freedom systems and their practical implications in vibration control.

1. Introduction

Electrical currents are induced in mechanical systems due to the interaction between motion and magnetic fields. They have been widely used as a means of mitigating vibrations in structural systems, with numerous implementations and studies conducted over the years [1–3].

A key challenge in incorporating induced current damping into mechanical systems lies in integrating the resulting electromagnetic or Lorentz forces into the dynamic system's equations of motion. This difficulty arises from the absence of analytical solutions for induced currents, necessitating numerical approaches such as finite element, finite differences, or finite volume methods, among others [4–6]. Consequently, the evaluation of velocity-dependent electromagnetic forces generally involves some degree of

* Corresponding author.
E-mail addresses: mikel.brun@opendeusto.es (M. Brun), fernando.cortes@deusto.es (F. Cortés), maria.elejabarrieta@deusto.es (M.J. Elejabarrieta).

https://doi.org/10.1016/j.jsv.2025.119550
Received 16 May 2025; Received in revised form 21 October 2025; Accepted 16 November 2025
Available online 17 November 2025

approximation. In the literature, these forces are typically represented within the equations of motion using matrices with linear, constant or frequency-dependent coefficients [7–9].

However, in a recent study by the authors, where induced currents were computed for a vibrating cantilever beam subjected to bending or torsional vibrations, it was observed that coupling between otherwise independent vibration modes arises when an external magnetic field is applied simultaneously in different directions [10].

To investigate this phenomenon in greater detail, a two-degree-of-freedom model is examined in this Rapid Communication as a preliminary step towards understanding the nature of mode coupling in more complex multi-degree-of-freedom systems incorporating induced current damping. The electromagnetic damping matrix derived from this model is non-proportional. Although non-proportional damping in mechanical systems is not novel and has been extensively studied over the years [11–13], it is novel in this specific context. In studies of induced current damping, it is common to approximate the velocity-dependent electromagnetic forces, and consequently, the influence of non-proportionality on the system dynamics is not examined. The insights gained here provide a foundation for extending the analysis to such systems in future studies.

2. Description of the system

The electromechanical system under consideration is illustrated in Fig. 1(a). It consists of a rectangular coil of length L in the x-direction and width b in the y-direction. The coil is fixed at its left side, while the right end is attached to elastic supports at each corner, each with stiffness k. The coil is placed in an external, uniform, time-invariant (i.e., static) magnetic field, denoted by $\mathbf{B}$, and is subjected to transverse vibrations characterised by the displacement vector $\mathbf{w}(x, y, t)$ indicated in Fig. 1(b). The external moments acting on the system are represented by $\mathbf{M}_{\text{ext}}(t)$.

The interaction between the vibrations and the magnetic field induces an electrical current $I(t)$ in the coil, which in turn generates an electromagnetic force per unit length $\mathbf{f}_{\text{em}}(t)$. To describe the electrical behaviour and determine the induced current, the coil is modelled as a purely resistive circuit with resistance R.

As shown in Fig. 1(b), the rectangular coil exhibits two degrees of freedom: a bending rotation about the y-axis at its fixed side,

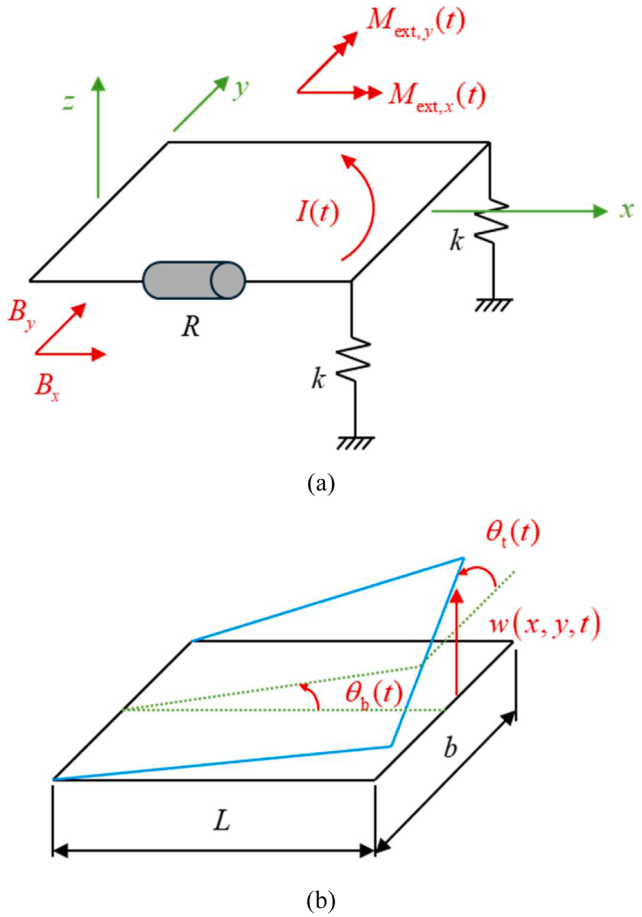

Fig. 1. Schematic representation of the coil vibrating in two directions in the presence of a static magnetic field: (a) overall model; (b) definition of the two degrees of freedom.

denoted by $\theta_b(t)$, and a torsional rotation about the x-axis at its right side, denoted by $\theta_t(t)$.

Specifically, the external magnetic flux density vector $\mathbf{B}$ is defined as

$$\mathbf{B} = B_x\hat{\mathbf{x}} + B_y\hat{\mathbf{y}}, \tag{1}$$

where B_x and B_y are its components in the x- and y-directions, respectively.

The transverse vibration of the coil is described by the displacement vector $\mathbf{w}(x,y,t) = w(x,y,t)\hat{\mathbf{z}}$, with the transverse displacement component $w(x,y,t)$ given by

$$w(x,y,t) = x\theta_b(t) + \frac{xy}{L}\theta_t(t). \tag{2}$$

The differential electromagnetic force, $d\mathbf{f}_{em}(t)$, generated by the induced current $I(t)$, is expressed using the Lorentz force as

$$d\mathbf{f}_{em}(t) = I(t)d\mathbf{l} \times \mathbf{B}, \tag{3}$$

where $d\mathbf{l}$ is a differential length vector and $\times$ denotes the cross product.

Finally, the external moments acting on the system are given by

$$\mathbf{M}_{ext}(t) = M_{ext,x}(t)\hat{\mathbf{x}} + M_{ext,y}(t)\hat{\mathbf{y}}, \tag{4}$$

where $M_{ext,x}(t)$ and $M_{ext,y}(t)$ are the components of the external moment in the x- and y-directions, respectively.

3. Dynamic equations of motion and electromagnetic damping matrix

The dynamic equations of motion for the coil depicted in Fig. 1 are given by

$$\mathbf{J}\ddot{\mathbf{q}}(t) + \mathbf{C}\dot{\mathbf{q}}(t) + \mathbf{K}\mathbf{q}(t) = \mathbf{M}_{ext}(t), \tag{5}$$

where $\mathbf{J}$ is the inertia matrix, $\mathbf{C}$ is the electromagnetic damping matrix, $\mathbf{K}$ is the stiffness matrix, $\mathbf{q}(t)$ is the generalised displacement vector defined as $\mathbf{q}(t) = [\,\theta_b(t) \quad \theta_t(t)\,]^T$ with $(\bullet)^T$ being the transpose operator, and $\dot{(\bullet)}$ denotes the time derivative.

From the kinetic energy of the system, the inertia matrix is obtained as

$$\mathbf{J} = \begin{bmatrix} J_b & 0 \\ 0 & J_t \end{bmatrix}, \tag{6}$$

where J_b and J_t are the mass moments of inertia associated with bending and torsional rotations, respectively.

From the potential energy of the system, the stiffness matrix is defined as

$$\mathbf{K} = \begin{bmatrix} k_b & 0 \\ 0 & k_t \end{bmatrix}, \tag{7}$$

where $k_b = 2kL^2$ and $k_t = kb^2/2$ are the stiffness coefficients associated with bending and torsional rotations, respectively. These values are related to the corresponding mass moments of inertia through $k_b = \omega_b^2 J_b$ and $k_t = \omega_t^2 J_t$, where ω_b and ω_t denote the natural angular frequencies of the uncoupled bending and torsional modes.

The electromagnetic damping matrix $\mathbf{C}$ is derived from the mechanical power dissipated by the induced electrical current $I(t)$. This power is given by

$$P_{mec}(t) = \sum_{i=1}^{4}\left(\int_{l_i} d\mathbf{f}_{em}(t)\cdot\dot{\mathbf{w}}(x,y,t)\right), \tag{8}$$

where $\cdot$ denotes the dot product, the index i refers to the four sides of the rectangular coil (numbered anticlockwise starting from the bottom), and l_i is the length of side i.

To evaluate Eq. (8), the induced current $I(t)$ must first be determined. The current arises due to motional induction, described by the general form of Faraday's law. Under the quasi-static assumption [14], neglecting self-induction effects and assuming a static magnetic field, Faraday's law applied to the circuit in Fig. 1(a) yields

$$I(t)R = \oint_C (\dot{\mathbf{w}}(x,y,t)\times\mathbf{B})\cdot d\mathbf{l}, \tag{9}$$

where C denotes the circuit path. Evaluating the contributions from each side gives

$$I(t) = \frac{Lb}{2R}\left(2B_x\dot{\theta}_b(t) + B_y\dot{\theta}_t(t)\right). \tag{10}$$

Substituting this current into the Eq. (8) yields a quadratic form

$$P_{\mathrm{mec}}(t) = -\frac{L^2 b^2}{4R}\left(4B_x^2\dot{\theta}_{\mathrm{b}}(t)^2 + 4B_xB_y\dot{\theta}_{\mathrm{b}}(t)\dot{\theta}_{\mathrm{t}}(t) + B_y^2\dot{\theta}_{\mathrm{t}}(t)^2\right), \tag{11}$$

where the negative sign indicates energy dissipation. As expected, this dissipated mechanical power is equal in magnitude to the Joule heating losses, $P_{\mathrm{Joule}}(t) = I(t)^2 R$.

Eq. (11) can be rewritten in matrix form as

$$P_{\mathrm{mec}}(t) = -\dot{\mathbf{q}}(t)^{\mathrm{T}}\mathbf{C}\dot{\mathbf{q}}(t), \tag{12}$$

with

$$\mathbf{C} = \frac{L^2 b^2}{4R}\begin{bmatrix} 4B_x^2 & 2B_xB_y \\ 2B_xB_y & B_y^2 \end{bmatrix}. \tag{13}$$

The electromagnetic matrix $\mathbf{C}$ is symmetric and non-proportional. In the case of a magnetic field applied solely along one direction, the system behaves as a purely dissipative system, analogous to viscous damping. However, when both components are present, coupling effects appear between bending and torsion, consistent with earlier observations [10]. Importantly, the off-diagonal terms arise only when the magnetic field has non-zero components in both the x- and y-directions. This coupling phenomenon will be analysed in more detail in Sections 4 and 5.

4. Analysis of the frequency response functions

This Section analyses the influence of both the magnitude and orientation of the external magnetic field on the modulus of the system's Frequency Response Functions (FRFs). The study specifically focuses on the amplitude of the resonance peaks at the undamped natural frequencies as a function of the magnetic field components, in order to reveal distinct dynamic behaviours associated with different coupling characteristics.

The FRFs of the system are derived from the receptance matrix $\mathbf{H}(\omega)$, which defines the relationship between the external harmonic moments and the system response. This matrix is obtained from the Fourier transform of Eq. (5), yielding

$$\mathbf{W}(\omega) = \mathbf{H}(\omega)\mathbf{M}, \tag{14}$$

where $\mathbf{W}(\omega)$ is the complex displacement amplitude vector, $\mathbf{M}$ is the moment amplitude vector, and $\mathbf{H}(\omega)$ is defined as

$$\mathbf{H}(\omega) = \left(-\omega^2\mathbf{J} + \mathrm{i}\omega\mathbf{C} + \mathbf{K}\right)^{-1}, \tag{15}$$

where $\mathrm{i} = \sqrt{-1}$ is the imaginary unit and $(\bullet)^{-1}$ denotes the matrix inverse. For the electromagnetic system under study, shown in Fig. 1, the receptance matrix $\mathbf{H}(\omega)$ is a 2×2 matrix given by

$$\mathbf{H}(\omega) = \begin{bmatrix} H_{\mathrm{bb}}(\omega) & H_{\mathrm{bt}}(\omega) \\ H_{\mathrm{tb}}(\omega) & H_{\mathrm{tt}}(\omega) \end{bmatrix}. \tag{16}$$

The four elements of this matrix represent the system's FRFs. To highlight the mode coupling effects, only the FRFs $H_{\mathrm{bb}}(\omega)$ and $H_{\mathrm{tb}}(\omega)$ are analysed, as the remaining terms lead to analogous conclusions. These two FRFs represent the response of the system to a unit amplitude bending moment M_{b}. Specifically, they are defined as $H_{\mathrm{bb}}(\omega) = W_{\mathrm{b}}(\omega)/M_{\mathrm{b}}$ and $H_{\mathrm{tb}}(\omega) = W_{\mathrm{t}}(\omega)/M_{\mathrm{b}}$, where $W_{\mathrm{b}}(\omega)$ and $W_{\mathrm{t}}(\omega)$ are the complex displacement amplitudes associated with bending and torsional rotations, respectively.

Table 1 presents the modulus of the FRFs $H_{\mathrm{bb}}(\omega)$ and $H_{\mathrm{tb}}(\omega)$ at the angular frequencies ω_{b} and ω_{t}, which correspond to the angular natural frequencies of the undamped, uncoupled modes associated with bending and torsional motions, respectively. It is worth noting that, upon close inspection of Table 1, the only FRF exhibiting an imaginary part at resonance is $H_{\mathrm{bb}}(\omega)$ at ω_{b}. It should also be noted that, if H_{tt} and H_{bt}, corresponding to a unit amplitude torsional moment M_{t} were analysed, analogous expressions would be obtained at the resonance frequencies to those of H_{bb} and H_{tb} in Table 1, but with the subscripts b and t interchanged. This would imply, for instance, that the only resonance frequency exhibiting an imaginary part would be H_{tt} at ω_{t}.

For the subsequent analysis, the coil length and width, along with the stiffness value of each spring, the electrical circuit resistance, and the mass moments of inertia associated with bending and torsion, are provided in Table 2. It is important to highlight that the mass

Table 1
Analytical expressions for the modulus of the FRFs $H_{\mathrm{bb}}(\omega)$ and $H_{\mathrm{tb}}(\omega)$ at the angular resonance frequencies ω_{b} and ω_{t}.

FRF	ω_{b}	ω_{t}
$\lvert H_{\mathrm{bb}}(\omega)\rvert$	$\lvert -\frac{B_y^2L^2b^2\omega_{\mathrm{b}} + 4\mathrm{i}J_xR\left(\omega_{\mathrm{b}}^2 - \omega_{\mathrm{t}}^2\right)}{4B_x^2J_xL^2\omega_{\mathrm{b}}\left(\omega_{\mathrm{b}}^2 - \omega_{\mathrm{t}}^2\right)}\rvert$	$\lvert \frac{1}{J_y\left(\omega_{\mathrm{b}}^2 - \omega_{\mathrm{t}}^2\right)}\rvert$
$\lvert H_{\mathrm{tb}}(\omega)\rvert$	$\lvert \frac{B_y}{2B_xJ_x\left(\omega_{\mathrm{b}}^2 - \omega_{\mathrm{t}}^2\right)}\rvert$	$\lvert -\frac{2B_x}{B_yJ_y\left(\omega_{\mathrm{b}}^2 - \omega_{\mathrm{t}}^2\right)}\rvert$

moments of inertia J_b and J_t have been selected such that the uncoupled resonance frequencies are $f_b = 20$Hz and $f_t = 30$Hz, respectively, considering that $\omega_b = 2\pi f_b$ and $\omega_t = 2\pi f_t$.

Two cases are considered, with the specific numerical values of B_x and B_y for each case provided in Table 3.

The FRFs are computed from Eq. (15) over a frequency range of 0–45 Hz with a resolution of 0.1 Hz, except near resonance peaks, where a finer resolution of 0.0001 Hz is used to capture the detailed behaviour.

Case 1

The modulus of the FRFs H_{bb} and H_{tb},both computed from Eq. (15), is shown in Figs. 2(a) and 2(b), respectively, for the case where B_y is held constant while B_x is varied.

The most significant observation is that the two degrees of freedom are clearly coupled. This is evidenced by the fact that the cross-FRF H_{tb} is non-zero across the entire frequency range, as shown in Fig. 2(b). This arises from the presence of a multi-directional magnetic field, which renders the off-diagonal terms of the electromagnetic damping matrix $\mathbf{C}$ non-zero. In the cross-FRF, two distinct resonance peaks can be clearly identified at f_b and f_t, whose values are consistent with the analytical expressions presented in Table 1.

However, despite the coupling observed in H_{tb}, only a single resonance peak appears in H_{bb} at f_b, with no additional peak at f_t, as shown in Fig. 2(a). The FRF remains essentially constant regardless of the magnetic field magnitude, in agreement with the analytical expressions for H_{bb} at f_t in Table 1. This behaviour occurs because no external torsional moment is applied; therefore, the coupling effect is captured exclusively in the cross-FRF H_{tb}.

The resonance peak of H_{bb} at f_b decreases with increasing B_x. This pronounced decrease is consistent with the analytical expression for the modulus of H_{bb} at f_b, since the modulus is inversely proportional to B_x^2.

Similarly, the resonance peak of H_{tb} at f_b decreases with increasing B_x. In contrast, the resonance peak at f_t increases with B_x. Although this contrasting trend may seem unexpected, it aligns with the analytical expressions in Table 1: H_{tb} is inversely proportional to B_x at f_b and directly proportional to B_x at f_t. Such contrasting peak behaviour in the cross-FRF H_{tb} cannot be captured in conventional induced-current damping models, where the electromagnetic damping matrix is often assumed to have constant or linearly varying coefficients and thus, it may lead to unforeseen system responses if this effect is not taken into account.

Finally, the modulus of H_{bb} remains largely unchanged outside the resonance frequency f_b as B_x increases. In contrast, the modulus of H_{tb} increases with B_x outside the resonance frequencies. This further underscores the complexity of the coupling mechanisms involved.

Case 2

The modulus of the FRFs H_{bb} and H_{tb}, both computed from Eq. (15), is shown in Figs. 3(a) and 3(b), respectively, for the case where B_x is fixed and B_y is varied.

As in Case 1, clear modal coupling is observed, as indicated by the non-zero cross-FRF H_{tb} in Fig. 3(b). Again, two distinct resonance peaks appear in H_{tb} at f_b and f_t, respectively, whereas only one resonance peak is present in H_{bb} at f_b. No additional peak appears in H_{bb} at f_t because no external torsional moment is applied, and therefore no coupling effect manifests in that FRF. Moreover, according to the analytical expression for H_{bb} at f_t in Table 1, the modulus remains constant regardless of the magnetic field magnitude.

The peak behaviour in both Figs. 3(a) and 3(b) is opposite to that observed in Case 1. Here, the peak of H_{bb} at f_b increases with B_y. The peak in the cross-FRF H_{tb} at f_b also increases, since it is directly proportional to B_y according to Table 1.

The resonance peak at f_t, however, decreases and eventually disappears for $B_y = 0.5$ T and $B_y = 1$ T, since, as indicated in Table 1, the modulus is inversely proportional to B_y. This implies that, although vibrations are strongly attenuated at f_t for large B_y, the vibration amplitudes at f_b become significantly higher for both degrees of freedom. Consequently, the coupling effect may lead to vibration amplification depending on the excitation frequency and on the magnitude and orientation of the external magnetic field.

Finally, as in Case 1, the modulus of H_{bb} in Fig. 3(a) shows negligible variation outside the resonance frequency f_b as B_y increases. By contrast, the modulus of H_{tb} tends to decrease with increasing B_y outside the resonances, except at very low frequencies, where the opposite trend is observed.

Table 2
System parameters.

Parameter	Value
L	200mm
b	10mm
k	12N/m
R	20mΩ
J_b	6.08×10^{-5}kg m^2
J_t	1.69×10^{-8}kg m^2

Table 3
Numerical values of B_x, and B_y for the analysed cases.

Case	B_x (T)	B_y (T)
1	0.1, 0.5, 1	0.1
2	0.1	0.1, 0.5, 1

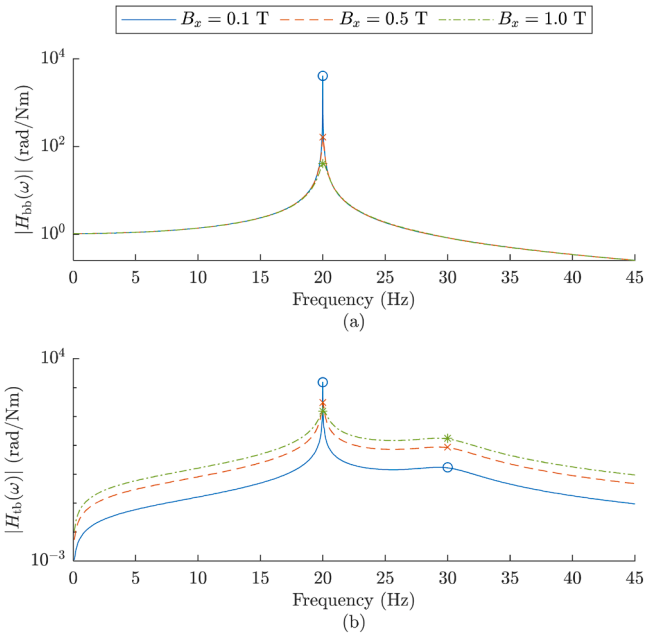

Fig. 2. Modulus of the FRFs for Case 1, with each plot highlighting a maximum at the resonance peaks for different values of B_x, while $B_y = 0.1$ T for all cases. The circle denotes the maximum for $B_x = 0.1$T (continuous line), the cross indicates the maximum for $B_x = 0.5$T (dashed line), and the asterisk marks the maximum for $B_x = 1$T (dotted line). Panels: (a) $|H_{bb}|$; (b) $|H_{tb}|$.

5. Analysis in the time domain

In this Section, a time-domain analysis is performed to visualise the transfer of energy between the two degrees of freedom of the system. The purpose of this analysis is to complement the frequency-domain analysis by providing a direct understanding of how energy exchange and attenuation occur over time. Specifically, the time evaluation of each degree of freedom is computed, together with the mechanical energies associated with them.

The time-domain response if obtained from Eq. (5) using the well-established Newmark integration method, whose formulation and numerical stability are extensively described in the literature [15].

For the subsequent analysis, the geometric and electromagnetic properties of the rectangular coil, together with the magnitudes of the external magnetic field components, are summarised in Table 4. Note that the mass moments of inertia J_b and J_t have been selected such that the uncoupled resonance frequencies are $f_b = 20$Hz and $f_t = 30$Hz, respectively, as was also imposed in the frequency-domain analysis.

The Newmark integration parameters are set to $\alpha = 0.25$ and $\beta = 0.5$. The response is computed for the case where the rectangular coil is subjected to an initial unit bending angle, while no initial torsional motion is applied. Hence, the initial conditions are defined as $\mathbf{q}(0) = [1 \quad 0]^T$ and $\dot{\mathbf{q}}(0) = [0 \quad 0]^T$. The time-domain response is calculated from $t = 0$s to $t = 0.33$s, using a time step of $\Delta t = 1\mu$s. The resulting time histories are presented in Fig. 4.

The behaviour of $\theta_b(t)$, shown in Fig. 4(a), reveals that the initial bending angle produces an oscillatory motion that is almost completely attenuated after just once vibration cycle. The amplitude after this first cycle is practically negligible compared with the initial deformation, demonstrating the strong electromagnetic damping effect introduced by the applied magnetic field.

Owing to the presence of a multi-directional magnetic field, a torsional oscillation is also induced in the system, as evidenced by the non-zero response of $\theta_t(t)$ in Fig. 4(b). This response starts from zero, since no initial torsional motion is applied, and arises purely due to the coupling between bending and torsion. The induced torsional oscillation decays more slowly than the bending component; while the amplitude of $\theta_b(t)$ decreases by approximately 87 % within the first cycle, $\theta_t(t)$ requires about eight cycles to experience a reduction of 72 %. This illustrates the different energy dissipation rates associated with each motion and highlights the influence of the coupling mechanism in redistributing energy between the two degrees of freedom.

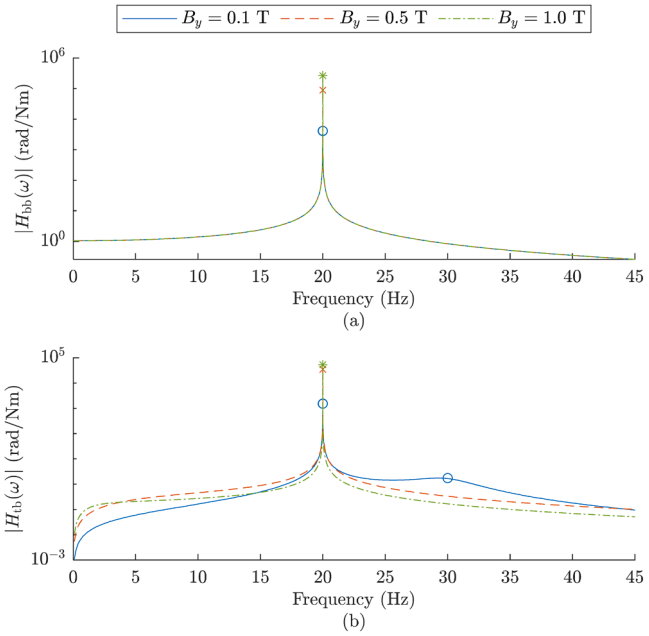

Fig. 3. Modulus of the FRFs for Case 2, with each plot highlighting a maximum at the resonance peaks for different values of B_y while $B_x = 0.1$ T for all cases. The circle denotes the maximum for $B_y = 0.1$T (continuous line), the cross indicates the maximum for $B_y = 0.5$T (dashed line), and the asterisk marks the maximum for $B_y = 1$T (dotted line). Panels: (a) $|H_{bb}|$; (b) $|H_{tb}|$.

Table 4
System parameters.

Parameter	Value
L	200mm
b	100mm
k	12N /m
R	20mΩ
J_b	6.08×10^{-5}kgm^2
J_t	1.69×10^{-6}kgm^2
B_x	0.5 T
B_y	0.1 T

The temporal evolution of the corresponding energies further supports this interpretation. As shown in Fig. 4(c), the total mechanical energy, initially at its maximum, decreases over time due to the electromagnetic damping forces. The decay rate varies, indicating intermittent energy exchange between bending and torsional modes.

The mechanical energy associated with $\theta_b(t)$ in Fig. 4(c) rapidly decreases, consistent with the electromagnetic damping effects, while the mechanical energy associated with $\theta_t(t)$ in Fig. 4(d) starts from zero, rises as energy transfers from bending, and then gradually decays. Eventually, both mechanical energies approach zero, confirming full dissipation through electromagnetic damping.

Overall, the time-domain results clearly demonstrate how the presence of multi-directional magnetic fields not only attenuates vibration amplitudes but also promotes complex energy exchange between coupled degrees of freedom. This dynamic interplay provides valuable insight into the transient response of the system and complements the frequency-domain analysis presented in Section 4.

6. Conclusions

A two-degree-of-freedom system comprising a rectangular coil subjected to bending and torsional motions in the presence of a static and uniform magnetic field has been analysed. The induced electromagnetic damping gives rise to a coupling effect between both degrees of freedom, represented by a symmetric electromagnetic damping matrix containing purely dissipative terms along its main diagonal and coupling terms in its off-diagonal entries. These coupling terms arise only when the magnetic field is multidirectional, introducing interactions that link the otherwise independent modal responses.

A combined frequency- and time-domain study has been conducted to characterise the modal coupling behaviour and to visualise the transfer of energy between the two degrees of freedom. The complementary nature of both analyses provides a comprehensive

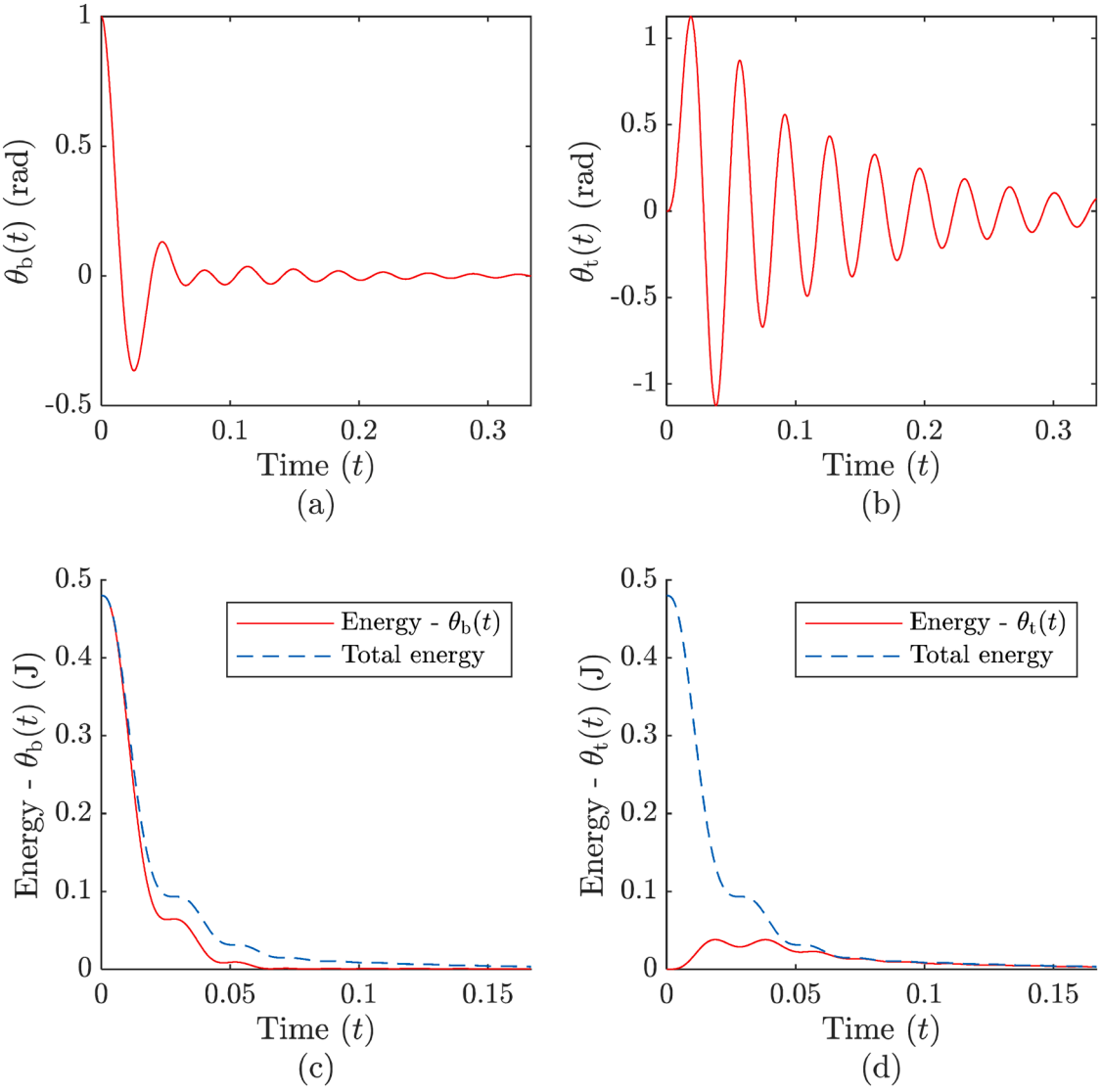

Fig. 4. Time domain response of the rectangular coil: (a) time-domain response of $\theta_b(t)$; (b) time-domain response of $\theta_t(t)$; (c) energy associated with $\theta_b(t)$; (d) energy associated with $\theta_t(t)$.

understanding of how electromagnetic damping influences the system dynamics.

In the frequency domain, the Frequency Response Functions (FRFs) of the system were evaluated for a harmonic moment bending excitation, focusing on H_{bb} and H_{tb}. The results showed that modal coupling occurs only when the magnetic field has components in multiple directions, since in that case the off-diagonal terms of the electromagnetic damping matrix become non-zero. This coupling manifests itself through the appearance of a non-zero FRF in the unexcited degree of freedom, indicating that energy is dynamically transferred between the two modes. Both analytical derivations and numerical simulations were carried out to determine the resonance amplitudes and their dependence on the magnitude and orientation of the magnetic field.

A particularly important finding is that increasing the magnetic field intensity can simultaneously attenuate vibration amplitudes in one mode while amplifying them in the other, depending on the field orientation.

In the time domain, the transient responses of both degrees of freedom were computed under an initial bending angle, together with the corresponding time histories of the associated mechanical energies. The results reveal that an initially pure bending motion induces a torsional response through the coupling mechanism, confirming the energy exchange predicted in the frequency-domain study. Although the bending oscillations are rapidly attenuated, the induced torsional oscillations decay more gradually, illustrating distinct dissipation rates for each mode. The total mechanical energy of the system gradually decreases due to the electromagnetic damping, while the redistribution of energy between bending and torsion is clearly observed over time.

Overall, the analysis presented offers a rigorous and insightful framework for understanding the dynamic response of systems with electromagnetic damping and coupled degrees of freedom. The combination of analytical expressions and numerical analysis provides

a solid foundation for extending this methodology to more complex configurations and lays the groundwork for future research into more complex multi-degree-of-freedom systems.

Declaration of generative AI and AI-assisted technologies in the writing process

During the preparation of this work the authors used ChatGPT in order to improve the language and readability of their paper. After using this tool, the authors reviewed and edited the content as needed and take full responsibility for the content of the publication.

CRediT authorship contribution statement

Mikel Brun: Writing – original draft, Software, Methodology, Formal analysis, Conceptualization. **Fernando Cortés:** Writing – review & editing, Supervision, Methodology, Formal analysis, Conceptualization. **María Jesús Elejabarrieta:** Writing – review & editing, Supervision, Methodology, Formal analysis, Conceptualization.

Declaration of competing interest

The authors declare that they have no known competing financial interests or personal relationships that could have appeared to influence the work reported in this paper.

Acknowledgements

This study has received financial support from the Department of Education of the Basque Government with the Research Group program IT1507–22.

Data availability

Data will be made available on request.

References

[1] E. Diez-Jimenez, R. Rizzo, M.-J. Gómez-García, E. Corral-Abad, Review of passive electromagnetic devices for vibration damping and isolation, Shock Vib. (2019) 1250707, https://doi.org/10.1155/2019/1250707, 2019.
[2] B.B. Shobhana, V.R. Panchal, V.A. Matsagar, Research developments of eddy current dampers for seismic vibration control of structures, J. Vib. Eng. Technol. 12 (2024) 5953–5971, https://doi.org/10.1007/s42417-023-01229-4.
[3] E.E. Kriezis, T.D. Tsiboukis, S.M. Panas, J.A. Tegopoulos, Eddy currents: theory and applications, Proc. IEEE 80 (1992) 1559–1589, https://doi.org/10.1109/5.168666.
[4] M. Passarotto, S. Pitassi, R. Specogna, Foundations of volume integral methods for eddy current problems, Comput. Methods Appl. Mech. Eng. 392 (2022) 114626, https://doi.org/10.1016/j.cma.2022.114626.
[5] J.R. Nagel, Finite-difference simulation of eddy currents in nonmagnetic sheets via electric vector potential, IEEE Trans. Magn. 55 (2019) 1–8, https://doi.org/10.1109/TMAG.2019.2940204.
[6] A. Alonso Rodríguez, E. Bertolazzi, R. Ghiloni, A. Valli, Finite element simulation of eddy current problems using magnetic scalar potentials, J. Comput. Phys. 294 (2015) 503–523, https://doi.org/10.1016/j.jcp.2015.03.060.
[7] H.A. Sodano, J.-S. Bae, D.J. Inman, W. Keith Belvin, Concept and model of eddy current damper for vibration suppression of a beam, J. Sound Vib. 288 (2005) 1177–1196, https://doi.org/10.1016/j.jsv.2005.01.016.
[8] J.-S. Bae, M.K. Kwak, D.J. Inman, Vibration suppression of a cantilever beam using eddy current damper, J. Sound Vib. 284 (2005) 805–824, https://doi.org/10.1016/j.jsv.2004.07.031.
[9] Z. Shi, J. Shan, C.N. Loong, W. Wu, C.-C. Chang, W. Shi, Experimental and numerical study on dynamic behavior of eddy current damping with frequency dependence, J. Eng. Mech. 146 (2020) 04020116, https://doi.org/10.1061/(ASCE)EM.1943-7889.0001852.
[10] M. Brun, F. Cortés, M.J. Elejabarrieta, Numerical analysis of energy dissipation due to eddy currents in a vibrating beam, J. Sound Vib. 595 (2025) 118787, https://doi.org/10.1016/j.jsv.2024.118787.
[11] F.E. Udwadia, A note on nonproportional damping, J. Eng. Mech. 135 (2009) 1248–1256, https://doi.org/10.1061/(ASCE)0733-9399(2009)135:11(1248).
[12] T. Kasai, M. Link, Identification of non-proportional modal damping matrix and real normal modes, Mech. Syst Signal Process. 16 (2002) 921–934, https://doi.org/10.1006/mssp.2001.1478.
[13] S. Mei, D. Cantero, C. Caprani, Evolution of modal properties in the non-proportionally damped coupled vehicle–bridge system, J. Sound Vib. 597 (2025) 118803, https://doi.org/10.1016/j.jsv.2024.118803.
[14] B.M. Notaroš, Total Electromagnetic Induction, Electromagnetics, Pearson, Upper Saddle River, NJ, 2011, pp. 289–294. International edition.
[15] K.-J. Bathe, Finite Element Procedures, Prentice Hall, 1996. Englewood Cliffs (N. J.).